Direct Numerical Simulation of Some Fundamental Problems Related to Transition in Laminar Separation Bubbles

Ulrich Rist, Ulrich Maucher, Siegfried Wagner [1]

Abstract. Direct Numerical Simulations of laminar separation bubbles are presented. The bubbles are generated by prescribing a locally decelerated free-stream velocity along a flat-plate. Controlled disturbances are introduced into the flow field upstream of the bubble by suction and blowing through the wall in order to study the linear and nonlinear stability characteristics of the flow. Two generic cases with different two-dimensional (*2-D*) and three-dimensional (*3-D*) initial disturbance amplitudes are investigated, a case (S) subject to secondary instability (strong amplification of *3-D* disturbances by resonance with a large amplitude *2-D* wave), and a *3-D* nonlinear case (O) where two oblique waves with opposite wave angle interact. After an initially very good agreement of the numerical results with primary and secondary instability it is found that the secondary instability in case (S) does not necessarily lead directly to *3-D* breakdown in contrast to the "oblique mechanism" in case (O) which is operative until saturation of the *3-D* disturbances. Recent results of the investigation of these mechanisms are presented, in addition to investigations of the effect of the wall on the instability of the flow. The possible occurrence of an absolute instability is also checked in a numerical simulation.

1 INTRODUCTION

Laminar separation bubbles occur due to boundary layer separation, transition, and turbulent reattachment of the flow. They can play a significant role in many flows of practical importance, as e.g., on laminar airfoils or turbine engine compressor blades, especially at low chord Reynolds numbers under changing flow conditions. The appearance and disappearance of separation bubbles leads to unsteady forces, which are difficult to predict when designing a new airfoil section.

[1] Institut für Aerodynamik und Gasdynamik der Universität Stuttgart , Pfaffenwaldring 21, 70550 Stuttgart, Germany

At present there exists a significant gap in our understanding of laminar-turbulent transition in a separated *2-D* boundary layer: separation and initial disturbance development is *2-D* but turbulence is inherently *3-D*, so, where, how, and why do *3-D* disturbances grow? Is turbulence in a *2-D* laminar separation bubble initiated by a sequence of instabilities like, for instance, in a flat-plate boundary-layer or more like in a free shear-layer, or is it due to absolute instability? Since it is very difficult to obtain *3-D* instantaneous flow-field measurements from experiments, Direct Numerical Simulations (DNS) of laminar separation bubbles based on the complete *3-D* Navier-Stokes equations can offer new insights.

In section 2 a brief overview of the numerical method being used is given. This is followed by a description of the base flow in section 3. Secondary instability and oblique wave interaction are discussed in section 4. The influence of the wall and the possibility of absolute instability are checked in sections 5 and 6, respectively. At the end, the results are summarized in section 7.

2 NUMERICAL METHOD

The success of a transition simulation strongly depends on the accuracy and the efficiency of the numerical method used. Compared to other CFD simulations, these requirements are typically orders of magnitude larger and attempts to use "standard CFD codes" for transition simulations (e.g., [8]) have failed so far.

The numerical method that we use is based on the vorticity-velocity formulation of the Navier-Stokes equations for incompressible unsteady flow [11]. Velocity components are denoted by u, v, and w in streamwise (x), wall normal (y), and spanwise direction (z), respectively (cf. Figure 1). The flow is split into a two-dimensional steady base flow and a three-dimensional unsteady disturbance flow in such a way that no linearization occurs. This makes the method more generally applicable for the investigation of transition phe-

nomena in different base flows without the need for altering the boundary conditions for the calculation of the disturbance flow from case to case.

Here, a closed laminar separation bubble in a Blasius boundary layer is calculated as base flow by prescribing a velocity distribution with local deceleration along the upper boundary BC of the integration domain, a technique already used by Gruber et al. [1]. Subsequently, small amplitude disturbances are introduced into the integration domain by timewise periodic blowing and suction upstream of the bubble, and their downstream development is calculated by solving the *3-D* disturbance flow equations.

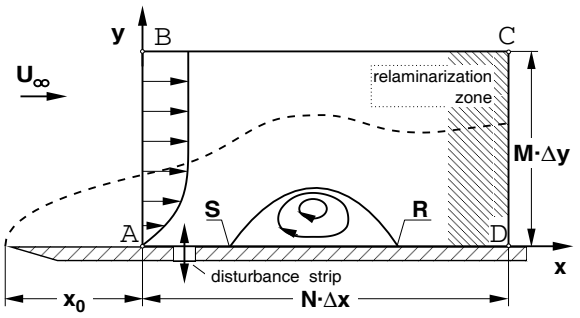

Figure 1. Integration domain for the DNS of a laminar separation bubble (**S:** separation, **R:** reattachment).

The boundary condition at the upper boundary of the integration domain allows for an exponential decay of the disturbances in y-direction, and hence using a relatively small integration domain. At the outflow boundary the disturbances are suppressed by direct manipulation of the disturbance vorticity in the so-called "relaminarization zone" upstream from the boundary [7].

Similar techniques called "buffer domains" or "fringe regions" [13] have been independently developed by different research groups all over the world [5]. They represent the current state-of-the-art for spatial transition simulation schemes and allow to exactly control the background disturbance-amplitude level which is essential to obtain grid-independent numerical results. We have carefully tested our technique and found that it works for boundary layers as well as for strongly non-parallel base flows, like for instance, free shear-layers or bluff-body wakes.

The equations are discretized assuming periodicity in spanwise direction only, and an efficient pseudo-spectral/finite difference scheme is constructed employing a Fourier ansatz in z-direction and fourth-order-accurate finite difference expressions in x- and y-direction. Efficiency is enhanced by using optimized Fast-Fourier-Transforms, multi-grid convergence acceleration and parallelization.

Time integration is performed by an explicit, fourth-order-accurate four stage Runge-Kutta scheme which is coupled with a hybrid discretization of the x-convection terms using central, upwind, downwind, and again central finite-differences in the four successive stages. The sequence of upwind and downwind differences is altered for every time step. It can be shown that this technique effectively damps out small-scale oscillations that cannot be accurately discretized on a given grid [6].

3 BASE FLOW

The integration domain $ABCD$ in Figure 1 extends from $x_0 = 0.37$ to $x_N = 5.06$ in downstream direction and from $y = 0$ to $y_M = 18.8$ normal to the wall. All variables are normalized by a constant reference length $L = 0.05m$ and by the free-stream velocity U_∞ at inflow. In addition, the y-direction and the vorticity are scaled by $\sqrt{Re}$ and $1/\sqrt{Re}$, respectively, where $Re = U_\infty L/\nu$ is the reference Reynolds number. $N = 697$ and $M = 96$ equally spaced intervals are used for the discretization of the flow field, except for case O which is discretized from $x_0 = 1.5$ to $x_N = 3.17$ using 437 intervals.

At the inflow boundary AB a Blasius boundary layer is specified with a local Reynolds number $Re_{\delta 1} = 330$ based on the displacement thickness. The velocity U_M at the free-stream boundary is specified by a fifth-order polynomial that matches continuously up to the second derivative with $u(y_M) = 1.0$ and $u(y_M) = 0.9$ up- and downstream of the bubble, respectively. This velocity distribution is shown in Figure 2 together with some results of the base-flow calculation.

Negative vorticity at the wall, between the separation and the reattachment point, indicates reverse flow inside the bubble, which is outlined by the separation streamline y_{sep}. The shape factor H computed from the boundary-layer velocity profiles indicates a rapid increase from the Blasius value $H = 2.59$ at inflow to rather high values inside the bubble, followed by an asymptotic relaxation back to the Blasius value downstream of the bubble. In this region the wall vorticity is nearly constant and somewhat lower than that for a Blasius boundary layer without a bubble starting at the same x_0 which is also presented in Figure 2.

4 UNSTEADY CALCULATIONS

Unsteady forcing at the wall is applied by specifying a finite wall-normal velocity within the disturbance strip located between $x_1 = 0.55$ and $x_2 = 0.70$. Periodic forcing with nondimensional frequency $f = 18$ ($F = 1.8$ in the standard instability diagram of a Blasius boundary layer) generates Tollmien-Schlichting (TS-) waves that travel downstream into the undisturbed flow. The disturbance frequency has been cho-

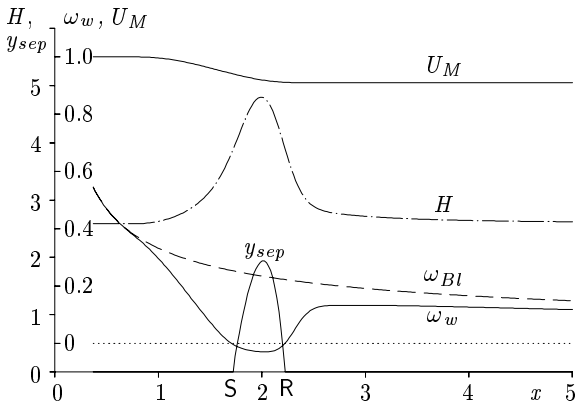

Figure 2. Base flow parameters: free-stream velocity U_M, shape factor H, separation streamline y_{sep}, wall vorticity ω_w and wall vorticity of a Blasius boundary layer ω_{Bl}. S = separation, R = reattachment point.

sen to correspond to the most amplified frequency for the steady base flow according to linear instability.

After simulation of several disturbance cycles, when the flow field becomes periodic, a Fourier analysis yields insight into the downstream growth of the corresponding disturbances which typically extends over several orders of magnitude of the amplitude. Two distinct cases are discussed in detail in the next two subsections, interaction of a large-amplitude *2-D* TS-wave with a small-amplitude *3-D* wave pattern of subharmonic frequency $f/2$, and the self interaction of two oblique waves with the same frequency and wave lengths but opposite flow direction in z-direction.

4.1 Case S, Secondary instability

Herbert[2] has developed a theory to describe the amplification of small-amplitude oblique waves in an approximately streamwise-periodic base flow that consists of the steady boundary layer profile ($u(y)$) and a finite-amplitude *2-D* TS-wave. The primary parameter of this so-called *secondary instability* is the amplitude of the *2-D* wave. As a rule of thumb, one may say that secondary instability occurs when this amplitude (measured as $A = u'_{max}/U_\infty$) exceeds $0.5 - 1\%$. The secondary amplification rate also depends on the spanwise wave number $\gamma = 2\pi/\lambda_z$ and on the frequency f of the *3-D* disturbances. Subharmonic *3-D* disturbances are usually most amplified for small A and fundamental ones for large A.

The rapid amplification of *3-D* disturbances by secondary instability leads to a rapid generation of higher harmonic disturbances in frequency and spanwise direction and to the final breakdown to turbulence by nonlinear interactions.

In [10, 12] we have already investigated secondary instabilities in the laminar separation bubble of the previous section and found that secondary amplification is hard to detect because it is only approximately twice as large as for primary instability. For comparison: in a Blasius boundary layer secondary amplification is typically one order of magnitude larger than the largest possible primary amplification rate.

In addition, we observed that the *3-D* disturbances exhibit a reduced amplification after saturation of the *2-D* primary wave. This phenomenon occurred for subharmonic, as well as for fundamental *3-D* disturbance frequencies [12].

Here we reconsider the subharmonic case S, where a *2-D* TS-wave with frequency $f = 18$ and a pair of *3-D* waves with frequency $f/2 = 9$ running in opposite oblique direction are introduced by periodic suction and blowing at the wall upstream of the bubble. The spanwise wave number of the subharmonic wave is $\gamma = 40$ which yields an oblique direction of about 60^o relative to the x-axis.

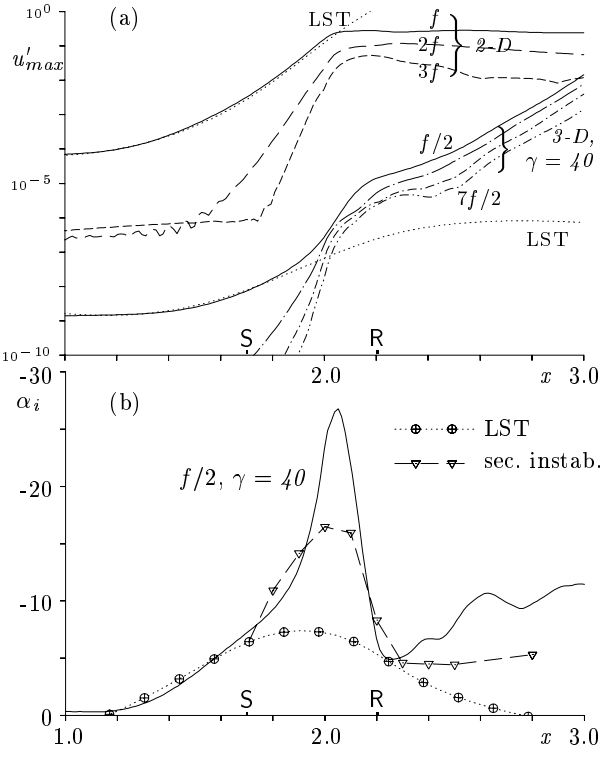

Figure 3. Comparison of the numerical results with linear stability theory (LST) and secondary instability theory. a) amplification curves, b) amplification rates. S = separation, R = reattachment of the undisturbed flow.

Amplification curves $u'_{max}(x)$ and amplification rates

$\alpha_i = -d/dx(\ln u'_{max})$ obtained after Fourier analysis of the numerical results from the 23^{rd} and 24^{th} fundamental disturbance period (i.e., the 12^{th} subharmonic disturbance cycle) are displayed in Figure 3. The *2-D* fundamental (f) and its higher harmonics ($2f$ and $3f$) are shown together with the *3-D* subharmonic ($f/2$) and its higher harmonics ($3/2f$, $5/2f$, and $7/2f$).

The downstream amplification of the *2-D* fundamental practically agrees with linear stability theory until its nonlinear saturation inside the bubble at $x \approx 2$. The higher harmonics of the *2-D* wave grow in a strikingly regular manner: for instance, when $u'_{max}(f) = 10^{-2}$, $u'_{max}(2f) = 10^{-4}$ and $u'_{max}(3f) \approx 10^{-6}$. Here, two-dimensional disturbances below 10^{-6}–10^{-7} cannot be observed due to numerical round-off errors.

The *3-D* subharmonic also grows like linear theory until $x \approx 1.8$, followed by a section with increased growth until $x \approx 2.2$ after which it reduces again. The higher harmonic *3-D* wave components are apparently generated by nonlinear interaction with the *2-D* fundamental: for instance, $(f/2, \gamma) + (f, 0) \mapsto (3/2f, \gamma)$, and so on. Thus, the distance between neighboring curves of the *3-D* spectrum in the downstream part of the flow field is approximately as large as the distance between the *2-D* fundamental and its first harmonic.

The growth rate of the *3-D*, $f/2$-disturbance is compared with results of linear stability and secondary stability theory in some more detail in Fig. 3b). The undisturbed base flow of section 3 has been used for the linear stability theory. The results therefore exhibit an increasing amplification rate until $x \approx 2$ followed by a decrease in the zone where the base flow relaxes back to a Blasius boundary layer.

For the secondary instability calculations, the local mean-velocity profile $\bar{u}(y)$ and fundamental *2-D* TS-wave amplitudes have been used. Figure 3b) shows that the increased *3-D* growth is due to secondary subharmonic resonance, as expected. However, the α_i-maximum around $x = 2.1$ is not predicted quantitatively very well. This might be due to strong nonparallel effects in the reattachment zone which have been neglected in the stability theory, but it could also be due to neglecting other *3-D* modes which have grown to the same order of magnitude as those considered in the theory. Downstream of the bubble, the theory also predicts a reduced amplification of the subharmonic compared to $x < 2.1$, as in the DNS.

Despite that only qualitative agreement with the results of the DNS is observed in the downstream part, it is obvious that *3-D* disturbances are still amplified in the "periodically modulated" *2-D* base flow. These disturbances are shown together with plots of the instantaneous (*2-D*) stream function and spanwise vorticity contours in Fig. 4. The *3-D* disturbance depicted by the contours $\pm 10^{-9}$, $\pm 10^{-8}$, ..., $\pm 10^{-4}$ radically changes its shape around $x \approx 2.0$: the local maxima and minima originating from the subharmonic wave are apparently "picked up" by the large-amplitude *2-D* disturbance. Thus, the wave length of the *3-D* disturbance adjusts to the *2-D* wave and the minima and maxima are torn around the centers of large-amplitude *2-D* vortices. This explains why the amplification in Figure 3a) suddenly changes when the *2-D* wave saturates.

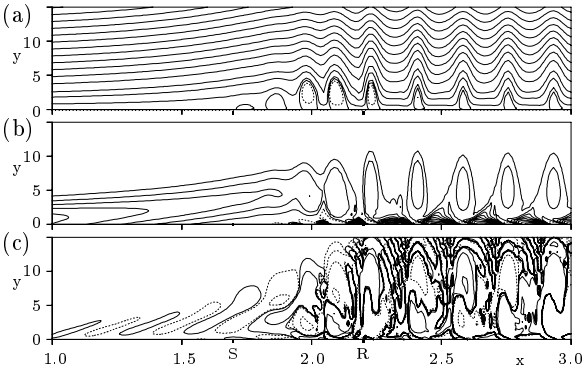

Figure 4. Instantaneous flow field for case S after 24 disturbance cycles. a) *2-D* stream function, b) *2-D* vorticity (contours: -0.06, 0.06, 0.12, ..., 0.9), c) z-component of *3-D* vorticity (contours: $\pm 10^{-9}$, $\pm 10^{-8}$, ..., $\pm 10^{-4}$). Negative contour lines are dashed.

4.2 Case O, Oblique breakdown

This part of our research is motivated by several observations: linear (primary) instability yields very large amplification rates in the separation bubble, the amplification of oblique waves with obliqueness angles under 30^o is approximately as large as that for *2-D* waves, and investigations such as the one discussed in the previous subsection have shown the possibility that *3-D* disturbance amplification by secondary instability does not necessarily lead directly to a turbulent flow in the separation bubble.

The so-called *oblique breakdown* starts from the nonlinear interaction of a pair of oblique waves of the same frequency running in opposite spanwise directions (forming a symmetric wave pattern). Higher harmonic wave components in spanwise and in frequency direction are rapidly built up, as can be seen in the amplification curves in Figure 5. Here, the initial behavior of the priming wave is again governed quite well by primary (linear) stability until nonlinear saturation of the disturbances. Additional simulations of this case have shown that the mechanism is most effective for the spanwise-wave-number–frequency combination shown here which corresponds to an obliqueness angle of approximately 20^o.

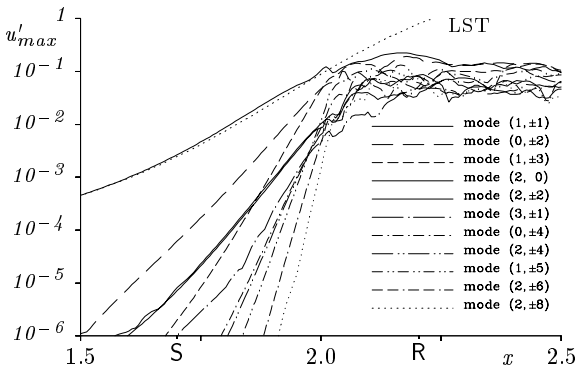

Figure 5. Amplification curves for *oblique breakdown*. Mode $(1, \pm 1)$: $f = 18$, $\gamma = \pm 20$, f = frequency, γ = spanwise wave number. LST = linear stability theory.

The instantaneous flow field is depicted in Figure 6 by contours of the *2-D* vorticity, the *3-D* vorticity component ω_z corresponding to $\gamma = 20$, and by the total z-vorticity at the wall. In contrast to Figure 4, a breakdown of the regular *3-D* wave pattern can be observed starting at $x \approx 2.0$ inside the boundary layer, i.e., below the phase shift of the *3-D* disturbances.

A staggered pattern is observed at the wall inside the bubble, but this does not indicate subharmonic breakdown here. In the absence of a large-amplitude *2-D* TS-wave this is merely a manifestation of the *3-D* oblique wave pattern.

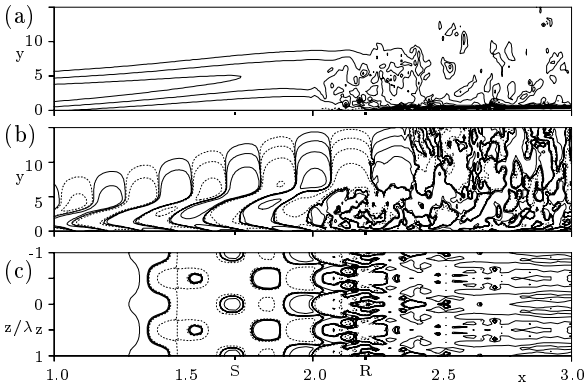

Figure 6. Instantaneous flow field for *oblique breakdown* after 22 disturbance cycles. a) *2-D* vorticity (contours: -0.06, 0.06, 0.12, ..., 0.9), b) z-component of *3-D* vorticity, c) z-component of vorticity at the wall. The contours in b) and c) are $\pm 10^{-5}$, $\pm 10^{-4}$, ..., $\pm 10^{0}$.

Downstream of the bubble, after the initial breakdown zone, longitudinal streaks appear. They belong to mode $(0,2)$ in the frequency–spanwise-wave-number–spectrum and they typically dominate the spectrum in all investigations of the oblique breakdown. The occurrence of longitudinal vortices in the reattachment zone has already been observed in wind-tunnel experiments (cf. [4]) but it has not yet been attributed to a possible oblique transition mechanism.

Figure 7 is intended for comparison with the subharmonic case of the previous section. Here, instantaneous spanwise vorticity contours are shown in streamwise cuts at $z = 0$. Case S is dominated by large-amplitude *2-D* disturbance waves which are stable, while case O shows a rapid formation of small-scale *3-D* structures in the reattached boundary layer.

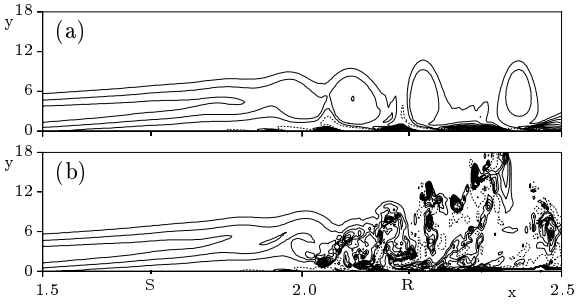

Figure 7. Comparison of instantaneous spanwise vorticity at $z = 0$ of case S (a) with case O (b).

5 INFLUENCE OF THE WALL

Here we want to investigate the influence of the wall on the primary (linear) *2-D* instability of the separated boundary layer. In literature about laminar separation bubbles it is usually argued that the separated flow behaves like a free shear-layer. With the data obtained in the DNS, some manipulation of the extracted base-flow profiles, and linear stability theory it is possible to investigate this hypothesis.

The u-velocity profile at $x = 2.0$, where the maximal reverse-flow occurs and where the bubble's height is largest, is taken as a starting position for these investigations. The first manipulation consists of shifting the profile in positive (u-) direction by the amount of the back flow ($\approx 1\%$) and setting the velocity between the minimum and the wall to zero. This has actually no significant influence on the linear instability and on the resulting eigenfunctions as can be seen in Figure 8 where both cases nearly coincide.

The next step consists of moving the shear layer further away from the wall by introducing additional grid points with zero velocity near the wall, as is shown in Figure 8a). The results indicate that the linear instability steadily approaches the typical instability curve

and eigenfunctions of a free shear-layer [9] when the wall distance is increased.

However, as can be seen in Fig. 8a) the wall distance that is needed to turn the present base-flow profile into a free shear-layer profile is rather large, and if one takes the relative importance of the near-wall maximum of the u'-eigenfunctions as a criterion, the base flow found in the DNS is far from a real free shear-layer and qualitative and quantitative comparisons with a free shear-layer should be regarded with care.

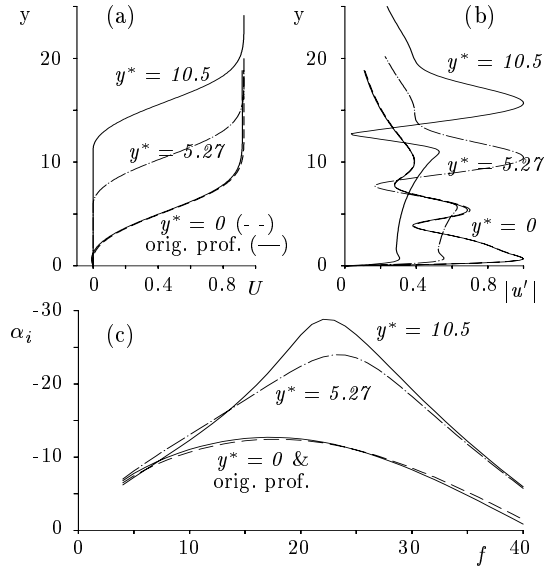

Figure 8. Investigation of the influence of the wall on the *2-D* linear instability of the separated boundary layer at $x = 2.0$. a) base flow profiles, b) u'-eigenfunctions, c) amplification rates versus frequency. y^* = additional distance at the wall with zero velocity.

6 ABSOLUTE INSTABILITY OF THE BASE FLOW

Flow fields with reverse-flow regions might be subject to absolute or global instability [3], i.e., there might be an amplification of disturbances which grow locally and which are not convected away by the oncoming flow. This will drive the flow to a new state which cannot be stopped by turning off the forcing of the disturbances. Here we want to investigate this possibility again by DNS in order to avoid possible ambiguities related to the neglection of nonparallel or other effects in an approximate theory.

The basic idea is to start from the subharmonic case shown in section 4.1 and to stop forcing at the wall after the 18^{th} disturbance cycle. If the flow were absolutely unstable, the disturbances arising from absolute instability would not decay because of zero or negative phase velocity. On the contrary, if they decay the flow is *convectively* unstable.

The results of our investigation are shown in Figure 9 by amplification curves for the fundamental *2-D* (a) and *3-D* disturbances (b) obtained after 30, 40, ..., 70 disturbance periods. Apart from a short-time increase of the *3-D* disturbance in the 30^{th} cycle which is due to the passage of a wave packet resulting from instantly turning off the disturbance strip, the harmonic disturbances die away on the long-term.

In the framework of the present investigation it could not be expected that all disturbances immediately disappear. It must be expected instead that it takes some time after stopping the forcing at the wall until they leave the integration domain in downstream direction. However, it is possible that other disturbances than those shown in Figure 9 remain. This possibility is checked in Figure 10 by the frequency spectra for the *2-D* and *3-D* disturbances at $x = 2.0$ and $x = 2.5$. The solid line shows the spectrum with forcing for comparison. It exhibits discrete peaks at the *2-D* fundamental, the *3-D* subharmonic, and their higher harmonic frequencies. The first spectrum, obtained from a Fourier analysis over ten subsequent fundamental disturbance periods after termination of the distrubance input still exhibits these peaks, but the space in-between is filled up due to the passage of the aforementioned wave packet. The third trace (p31–40) is as a whole very high due to this, especially at $x = 2.5$.

In the later periods all disturbances gradually decrease, indicating that the base flow considered here must be *convectively unstable*. However, two peculiarities can be observed: a slower decay of the convectively unstable *2-D* Tollmien-Schlichting waves in a band centered around $f = 18$, and the rather slow decay of the longitudinal vortices ($f \to 0$) in the *3-D* spectrum.

7 CONCLUSIONS

The investigations of secondary instability discussed here have shown that the largest *3-D* amplification occurs just prior to nonlinear saturation of the *2-D* wave. After this the *3-D* amplification is reduced so that the flow field remains dominated by large-amplitude *2-D* vortices which seem to redistribute the *3-D* disturbance field in such a way that the initial eigenmodes completely disappear.

The investigation of the most unstable oblique case revealed a rapid breakdown of the flow in contrast to the subharmonic case. The influence of the wall on the linear *2-D* instability appears to be important: compared to a free shear-layer, the maximal amplification rate is considerably reduced and the eigenfunctions present a large near-wall maximum. Finally, absolute instability could not be found, since all disturbances decayed after termination of the forcing at the wall.

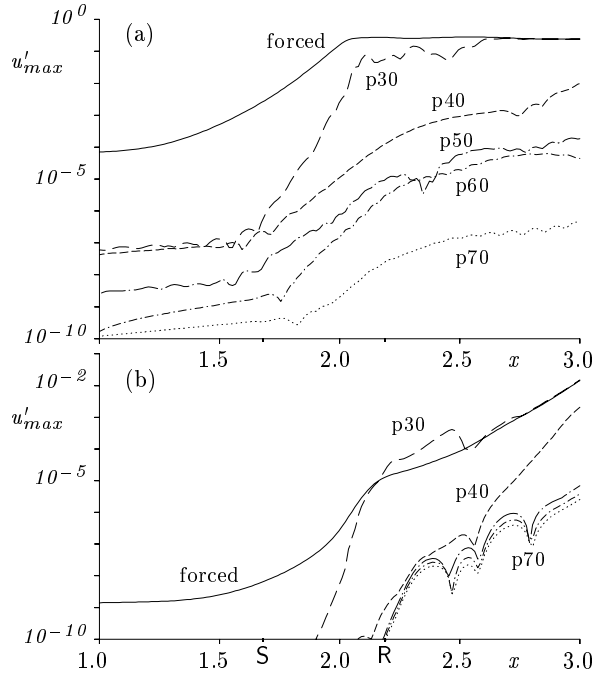

Figure 9. Amplification curves of u'_{max} after termination of the disturbance input compared to the forced periodic results of Fig. 3a). a) *2-D* disturbances, frequency f, b) *3-D* disturbances, subharmonic frequency $f/2$, $\gamma = 40$. p30 = 30^{th} disturbance period, etc.

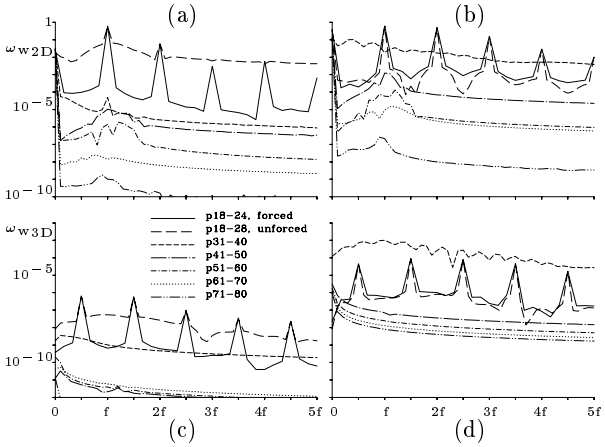

Figure 10. Frequency spectra of the wall vorticity after termination of the disturbance input in the 25^{th} cycle. a) *2-D*, $x = 2.0$, b) *2-D*, $x = 2.5$, c) *3-D*, $x = 2.0$, d) *3-D*, $x = 2.5$

8 ACKNOWLEDGEMENTS

This research is supported by the Deutsche Forschungsgemeinschaft, Bonn-Bad Godesberg (DFG) and by the University of Stuttgart.

REFERENCES

[1] K. Gruber, H. Bestek, and H. Fasel. *Interaction between a Tollmien-Schlichting wave and a laminar separation bubble*, AIAA-paper 87-1256, 1987.

[2] T. Herbert, *Secondary instability of boundary layers*, volume 20 of *Annual Review of Fluid Mechanics*, 487–526, Annual Reviews Inc., Palo Alto, CA, 1988.

[3] P. Huerre and P.A. Monkewitz, *Local and global instabilities in spatially developing flows*, volume 22 of *Annual Review of Fluid Mechanics*, 473–537, Annual Reviews Inc., Palo Alto, CA, 1990.

[4] G.R. Inger. *A theoretical study of spanwise-periodic 3-D disturbances in the wake of a slightly stalled wing at low Reynolds numbers*, Proc. *Aerodynamics at Low Reynolds numbers* $10^4 < Re < 10^6$, Internat. Conf., Royal Aeronautical Society, London, Oct., 1986.

[5] L. Kleiser and T.A. Zang, *Numerical Simulation of Transition in Wall-Bounded Shear Flows*, volume 23 of *Annual Review of Fluid Mechanics*, 495–537, Annual Reviews Inc., Palo Alto, CA, 1991.

[6] M. Kloker. *Direkte Numerische Simulation des laminar-turbulenten Strömungsumschlages in einer stark verzögerten Grenzschicht*, Dissertation Universität Stuttgart, 1993.

[7] M. Kloker, U. Konzelmann, and H. Fasel, 'Outflow boundary conditions for spatial Navier-Stokes simulations of transitional boundary layers', *AIAA Journal*, **31**, 620–628, (1993).

[8] E. Laurien, *On the numerical simulation of spatial disturbances in a blunt-nose flat plate flow*, 443–447, Instability and Transition, ICASE/NASA LaRC Workshop 1989, Springer, Berlin, New York, 1990.

[9] A. Michalke, 'On spatially growing disturbances in an inviscid shear layer', *Journal of Fluid Mechanics*, **23**, 521–544, (1965).

[10] U. Rist, *Nonlinear effects of 2-D and 3-D disturbances on laminar separation bubbles*, 330–339, IUTAM-Symposium on Nonlinear Instability of Nonparallel Flows, Clarkson University, Potsdam, NY, USA, Springer, Berlin, New York, 1994.

[11] U. Rist and H. Fasel, 'Direct numerical simulation of controlled transition in a flat-plate boundary layer', *Journal of Fluid Mechanics*, **298**, 211–248, (1995).

[12] U. Rist and U. Maucher, *Direct Numerical Simulation of 2-D and 3-D instability waves in a laminar separation bubble*, 34–1 – 34–7, Application of Direct and Large Eddy Simulation to Transition and Turbulence, AGARD–CP–551, Chania, Crete, 1994.

[13] P.R. Spalart and J.H. Watmuff, 'Experimental and numerical study of a turbulent boundary layer with pressure gradients', *Journal of Fluid Mechanics*, **249**, 337–371, (1993).